Geometry, Mechanics, and Electronics of Singular Structures and Wrinkles in Graphene

Vitor M. Pereira and A. H. Castro Neto*
Department of Physics, Boston University, 590 Commonwealth Avenue, Boston, Massachusetts 02215, USA
H. Y. Liang and L. Mahadevan*
School of Engineering and Applied Sciences, Harvard University, 29 Oxford Street, Cambridge, Massachusetts 02138, USA
(Received 12 May 2010; published 5 October 2010)

As the thinnest atomic membrane, graphene presents an opportunity to combine geometry, elasticity, and electronics at the limits of their validity. We describe the transport and electronic structure in the neighborhood of conical singularities, the elementary excitations of the ubiquitous wrinkled and crumpled graphene. We use a combination of atomistic mechanical simulations, analytical geometry, and transport calculations in curved graphene, and exact diagonalization of the electronic spectrum to calculate the effects of geometry on electronic structure, transport, and mobility in suspended samples, and how the geometry-generated pseudomagnetic and pseudoelectric fields might disrupt Landau quantization.

DOI: 10.1103/PhysRevLett.105.156603 PACS numbers: 72.80.Vp, 61.48.Gh, 62.20.−x

Graphene wrinkles easily and often [1]. That is most clear in samples exfoliated from graphite [2], or in chemically derived oxides [3]. Since graphene is an atomically thin membrane, it is impossible to lay a shear-free sheet of it onto a flat surface, as it sticks almost immediately to a substrate—such as the edges of a trench via van der Waals interaction—and the substrate is itself rarely, if ever, flat [4–6], so that perfect shear-free conformations are not possible. Recently developed techniques to grow graphene on metallic surfaces also show widespread wrinkling from thermal expansion mismatch between graphene and the host [7,8]. These boundary deformations acting on graphene lead to wrinkling because of the nearly negligible threshold for buckling instabilities in thin plates and membranes, which cannot support even arbitrarily small shear or compression without wrinkling on scales large compared to its thickness [9].

For all its flexural limpness, graphene exhibits the largest in-plane Young's modulus [10] and, though easy to bend, is extremely hard to stretch. This geometry-induced separation of the energy scales for thin membranes implies that they try to respond to shear by bending isometrically almost everywhere [11]. However, except in very limited cases corresponding to developable deformations, bending alone cannot accommodate the state of stress or the boundary conditions imposed by the geometry. This conflict is resolved naturally by local membrane stretching by an amount sufficient to just accommodate the imposed geometric and physical constraints, so that regions of in-plane strain are restricted to vanishingly small areas distributed throughout the system. A simple example is seen in a thin sheet of paper which is very resistant to stretching (it actually tears before we can stretch it), but bends easily; when a piece of crumpled paper is straightened out, we see flat areas connected by a network of ridges that meet at sharp vertices: the highly localized scars where the sheet is plastically deformed. The peaked structures constitute the basic element of the entire ridge network, and serve to focus large strains and energy densities. They are ubiquitous in thin films that are strongly deformed in such instances as drapes [11], skin wrinkles, etc., and are termed developable cones or conical singularities (CSs); their outer form has been geometrically and mechanically characterized in terms of a theory for the inextensional deformations of thin sheets, Refs. [12,13]. In particular, there is a simple universal analytic expression for their geometry as a function of the boundary and/or stress conditions on the sheet far from the nearly singular tip where the effects of stretching are concentrated.

Exfoliated graphene and suspended samples [2] naturally exhibit CSs as shown in Fig. 1(a), which are of particular interest in the quest for ultimate electronic mobility [14,15] and nontrivial interaction effects [16,17]. Here study the influence of these ubiquitous objects on electronic transport in graphene. Unlike in most solid-state materials, flexural and planar deformations couple to electrons in graphene in a peculiar way due to their Dirac nature [18]. Strain in the carbon lattice couples to these excitations through both effective gauge fields, and local scattering potentials, that follow the local curvature and thus affect the electronic structure [19,20], often in striking ways [21,22]. CSs are also present in buckled nanotubes, where they have been shown to significantly alter transport characteristics [23].

Conical singularities.—Graphene does behave like a thin plate under stress, even at the atomistic level; when sheared biaxially, and afterwards allowed to relax via molecular dynamics (MD) [24], Fig. 1(c) shows the relaxed configuration, which exhibits the classical Miura-ori like ridge pattern of 2D buckling [25], with the CSs arising at the intersection of the ridges Figs. 1(e) and 1(f).

In cylindrical coordinates, the displacement field associated with the CSs, a generalized cone, reads

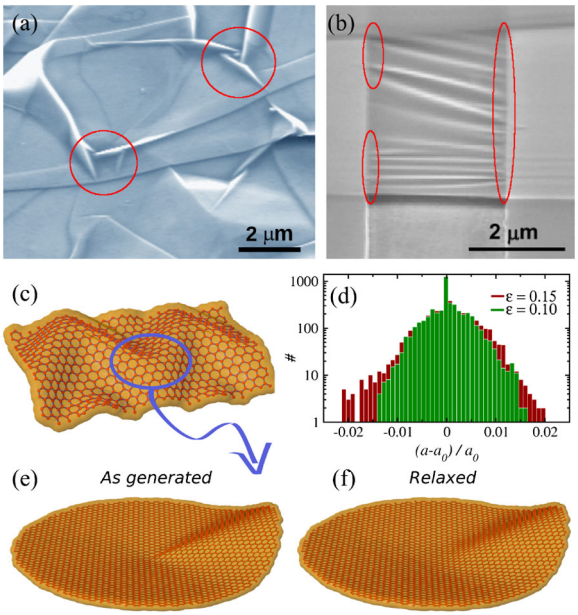

FIG. 1 (color online). (a) Folded graphene sheet resembling the draping of a textile, and graphene suspended over a trench, (b) [35]. Some regions with visible CSs are highlighted. (c) Relaxed atomistic profile of a portion of graphene under biaxial shear, displaying typical buckling ridges. (d) log-histogram of the interatomic distances in the relaxed configuration (f) for two values of ε. (e),(f) Profile of the CSs studied here ($\varepsilon = 0.1$). The atomic positions are shown as generated by applying $\boldsymbol{u}(\rho, \theta)$ to all atoms, (e), and after relaxation by MD, (f).

$\boldsymbol{u}(\rho, \theta) = \boldsymbol{r} - \boldsymbol{r}_0 = u_\rho(\rho, \theta)\boldsymbol{u}_\rho + u_\theta(\rho, \theta)\boldsymbol{u}_\theta + \zeta(\rho, \theta)\boldsymbol{z}$, where $\zeta(\rho, \theta) = \rho\,\psi(\theta)$. The solution for $u_\theta(\rho, \theta)$, $u_\rho(\rho, \theta)$, and $\psi(\theta)$ is obtained by solving the equations of equilibrium for the finite bending of a plate with the constraint of inextensibility, i.e., that there is no in-plane strain ($\gamma_{ij} = 0$). The vertical displacement is then given by $\zeta = \rho\,\psi(\theta)$ (Refs. [12,24])

$$\psi(\theta) = \varepsilon\Theta(|\theta| - \theta_1) + \varepsilon\Psi(\theta)\Theta(\theta_1 - |\theta|), \qquad (1)$$

where ε characterizes the angle of the enveloping cone, and both $\theta_1 \approx 70°$ and $\Psi(\theta)$ are universal. This independence of the shape on any material parameters and scale, together with the Cauchy-Born hypothesis, allows us to describe conical singularities and wrinkling in graphene by applying the deformation field $\boldsymbol{u}(\rho, \theta)$ to all atoms in the lattice. The resulting shape of the lattice is the one shown in Fig. 1(e), with the main effects arising from curvature. Since $\boldsymbol{u}(\rho, \theta)$ is constructed so that there is no in-plane strain; however, some localized stretching strain is concentrated in the neighborhood of the apex which will relax naturally in a MD simulation as a consequence of the large but finite stretching rigidity of graphene so that, even after relaxation, all interatomic distances are strongly peaked about the natural lattice spacing $a = a_0 = 1.42$ Å, as can be seen in Fig. 1(d), with a spread of 2% for the values of ε of interest here. This is just a reflection of the relative inextensibility of the in-plane σ bonds, which leads to a blunting of the apex but is of little significance elsewhere. Since the relaxed structure shows strain >1% for a dozen of atoms only, and very near the apex, we shall neglect it altogether.

Effective model.—To understand how the electronic properties respond to this deformation, we note that the relevant physics occurs in the p_z-derived π bands of graphene; curvature causes rehybridization of these orbitals [26], hindering or favoring wave function overlap, and thus perturbs the electronic kinetic energy. This affects both the π band subsystem and hybridizes the p_z and the sp^2 sub-bands, which are otherwise orthogonal. As a first step we shall neglect this latter effect, which mostly shifts the chemical potential, and focus only on the π bands.

Within the tight-binding approximation, the band structure is then determined by the effective Hamiltonian

$$H = \sum_{\langle i,j\rangle} t_{ij} c_i^\dagger c_j + \sum_{\langle\langle i,j\rangle\rangle} t'_{ij} c_i^\dagger c_j + \text{H.c.}, \qquad (2)$$

where the two contributions come from first and second neighbors, and $t_{ij}^{(\prime)} = V_{pp\pi}$ is the two center Slater-Koster overlap integral, which has to be calculated now for all pairs of neighbors, taking into consideration the full geometry of the deformed lattice. To do this, we introduce the unit normal at every point of the surface, $\boldsymbol{n}(\rho, \theta)$, so that for two atoms separated by an arbitrary distance $\boldsymbol{d} = \boldsymbol{R}_i - \boldsymbol{R}_j$, straightforward rotation of the p_z orbitals and Slater-Koster tables tell us that the overlap integral is [27]

$$t_{ij} = V_{pp\pi}\boldsymbol{n}_i \cdot \boldsymbol{n}_j + (V_{pp\sigma} - V_{pp\pi})(\boldsymbol{n}_i \cdot \hat{\boldsymbol{d}})(\boldsymbol{n}_j \cdot \hat{\boldsymbol{d}}). \qquad (3)$$

Since the surface is completely parametrized by the normal displacement field, we may use the geometry of the developable cone to obtain the normals, distances and the hopping t_{ij} among any two atoms, noting that the underlying metric remains Euclidean. To make progress analytically we assume [28], $d^2 V_{ppx}(d) = d_0^2 V_{ppx}(d_0)$, so that on solving the Gauss equations we obtain $t_{ij}(\boldsymbol{d}) = t_{ij}^0(\boldsymbol{d}_0) + \delta t_{ij}$, with

$$\delta t_{ij} \approx -V_{pp\pi}^0 \frac{1}{2}|(\boldsymbol{d}_0 \cdot \boldsymbol{\nabla})\boldsymbol{\nabla}\zeta|^2 + \frac{V_1}{d_0^2}[(\boldsymbol{d}_0 \cdot \boldsymbol{\nabla})^2\zeta]^2, \qquad (4)$$

$V_1 = V_{pp\pi}^0/3 - V_{pp\sigma}^0/4$. In the low energy approximation, we may then describe (2) by the effective Dirac Hamiltonian: $H \approx v_F\boldsymbol{\sigma} \cdot [\boldsymbol{p} - \frac{1}{v_F}\mathcal{A}(\boldsymbol{r})] + [3t'_0 + \Phi(\boldsymbol{r})]\sigma^0$ in each valley of the Brillouin zone. Then the effective gauge field $\mathcal{A}(\boldsymbol{r})$ and the local potential $\Phi(\boldsymbol{r})$ depend, respectively, on the perturbations of the nearest neighbor, and next-nearest neighbor hopping Ref. [18] via

$$\mathcal{A}_x - i\mathcal{A}_y = \sum_{\boldsymbol{n}} \delta t_{\boldsymbol{n}}(\boldsymbol{r}) e^{i\boldsymbol{k}\cdot\boldsymbol{n}}, \qquad \Phi = \sum_{\Delta} \delta t'_\Delta(\boldsymbol{r}) e^{i\boldsymbol{k}\cdot\boldsymbol{\Delta}}. \qquad (5)$$

Substituting (4) in (5), one obtains

$$\Phi(\boldsymbol{r}) = \alpha\,\mathrm{Tr}^2[\partial^i\partial_j\zeta] - \beta\det[\partial^i\partial_j\zeta], \qquad (6)$$

with $\alpha = 9a_0^2V_{pp\pi}^0/8 + 27a_0^2V_{pp\sigma}/32 \approx 1.5$ eV Å^2, and $\beta = 3a_0^2V_{pp\pi}^0 + 9a_0^2V_{pp\sigma}^0/8 \approx 3$ eV Å^2 [29]. We recall that $\partial^i\partial_j\zeta \approx K^i{}_j$ is the curvature tensor of our conical

surface and, since $H = \mathrm{Tr}K^i{}_j/2$ and $\det K^i{}_j$ are the local mean and Gaussian curvatures, it follows that Φ is entirely determined by the cone geometry. Moreover, since CSs are developable surfaces, the Gaussian curvature vanishes everywhere, so that $\Phi(\boldsymbol{r}) = \alpha a_0^2(\nabla^2\zeta)^2$. The gauge field $\mathcal{A}$ is also given in terms of products of $\partial^i\partial_j\zeta$, but we shall not write it explicitly since this potential couples to the electric current, and therefore does not contribute in leading order for scattering and transport when time-reversal symmetry is preserved. However, Φ leads to an electrostatic potential that is felt by the Dirac electrons and thus contributes directly to the resistivity.

Transport.—We now consider the contribution of the CSs for the momentum relaxation time in the Boltzmann formalism. In the Born approximation, the scattering rate is given by $S(\boldsymbol{k}, \boldsymbol{k}') = 2\pi/\hbar|V_{\boldsymbol{k},\boldsymbol{k}'}|^2\delta(E_{\boldsymbol{k}} - E_{\boldsymbol{k}'})$, with $V_{\boldsymbol{k},\boldsymbol{k}'} = \Phi_{\boldsymbol{k}-\boldsymbol{k}'}[1 + \exp(i\phi_{\boldsymbol{k}} - i\phi_{\boldsymbol{k}'})]/2$, and $\Phi_{\boldsymbol{q}}$ is the Fourier transform of the local potential (6): $\Phi(\boldsymbol{r}) = \alpha a_0^2[\psi(\theta) + \psi''(\theta)]/r^2$, which is of course directly related to the cone geometry. This potential is unusual for two reasons: it is anisotropic on account of (1) and decays in space as $\propto 1/r^2$, so that it is beyond the supercritical threshold for Dirac fermions in 2D [30]. Were it not for the natural lattice regularization at $r \sim 0$, such potential would lead to an unbound spectrum of discrete states. This effect is also blunted by the mechanical relaxation observed near the apex in Figs. 1(e) and 1(f). The result is a short range potential with a finite number of bound states (unlike the Coulomb case where the long range $1/r$ tail begets an infinite spectrum of resonances, even after regularization), so that CSs therefore scatter as short range, anisotropic potentials.

The $1/r^2$ decay in the potential leads to an infrared divergence in $\Phi_{\boldsymbol{q}}$ with a leading order isotropic contribution $\Phi_{\boldsymbol{q}} \approx -10\alpha\varepsilon^2\log(qr_0)$, all anisotropy being hidden in the subleading terms, with the regularization distance, r_0 of the order of the lattice spacing, reflecting the relaxation in the neighborhood of the apex. Then, the CSs scatter primarily as an isotropic $1/r^2$ potential, and the scattering time for the potential ν_0/r^2 can be calculated exactly, and reads

$$\frac{1}{\tau(k_F)} = \frac{2\pi^2 n_i \nu_0^2}{v_F\hbar^2} k_F G^{3,1}_{2,4}\left(4k_F^2 r_0^2 \,\middle|\, \begin{matrix} -\frac{1}{2}, \frac{1}{2} \\ 0, 0, 0, -2 \end{matrix}\right), \tag{7}$$

where G is a Meijer function [31], n_i the density of scatterers, and k_F relates to the carrier density via $k_F^2 = \pi n_e$. Then the longitudinal conductivity follows from Eq. (7) and yields

$$\sigma = \sigma_0 G^{3,1}_{2,4}\left(4k_F^2 r_0^2 \,\middle|\, \begin{matrix} -\frac{1}{2}, \frac{1}{2} \\ 0, 0, 0, -2 \end{matrix}\right)^{-1}, \qquad \sigma_0 = \frac{v_F^2\hbar e^2}{2\pi^3 n_i \nu_0^2} \tag{8}$$

which is only relevant in the regime $0 < kr_0 \lesssim 1$ shown in Fig. 2. We see that the conductivity is essentially *linear in electron density* throughout most of the region of interest, except for the logarithmic singularity around the Dirac point,

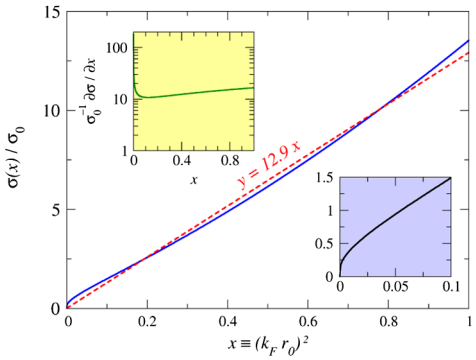

FIG. 2 (color online). dc conductivity (8) versus the adimensional electron density $x \equiv (k_F r_0)^2$. Dashed line shows the best linear fit in the entire domain. Top inset shows $\sigma_0^{-1}\partial\sigma/\partial x$, which is how the electronic mobility (μ) is frequently extracted experimentally. Bottom inset amplifies the region $k_F \sim 0$, dominated by a log singularity.

where it grows sublinearly. The corresponding approximate mobility is $\mu \approx \frac{6v_F^2\hbar e r_0^2}{\pi^2\nu_0^2}\frac{1}{n_i}$, and when ν_0 is replaced by the corresponding parameter for CSs ($\nu_0 \to 67\alpha\varepsilon^2/\pi$ eV Å^2) one obtains the mobility for a set of uncorrelated CSs as $\mu \approx 10^{29} r_0^2/(n_i\varepsilon^4)$ cm^2/(Vs). Substituting the parameter values $r_0 \sim 5$ Å and $n_i \sim 10^{12}$ cm^{-2}, results in $\mu \sim 10^3/\varepsilon^4$cm^2/(Vs). The ε^4 dependence reflects a strong sensitivity to the aperture of the enveloping cone of each CS, but given that $\varepsilon \lesssim 0.5$, it causes relatively small scattering. This effect should thus be more important in high- mobility suspended samples, where the CSs can become a limiting factor in carrier mobility.

Electronic spectrum.— Although the gauge fields $\mathcal{A}$ are not expected to contribute to transport at leading order, they do influence the electronic spectrum. In fact, since they arise from perturbations to nearest neighbor hopping, they might cause considerable fictitious magnetic fields [22]. To address this at the level of the lattice, we have calculated the electronic structure associated with the full tight-binding Hamiltonian (2) in the presence of a single unrelaxed CS. The local density of states [LDOS, $N_{\boldsymbol{r}}(E)$] for representative parameters is shown in Fig. 3. We see that CSs scatter strongly enough to create bound electronic states as shown in Figs. 3(a)–3(c) by the sharp peaks for states beyond the band edge, decaying rapidly away from the apex. In addition, the LDOS is very structured at other energies within the band, signaling the formation of resonant states. This is more clearly visible in Fig. 3(c) where the sampling points lie in the region of higher curvature. In this case the LDOS curves show even stronger perturbation around the Dirac point. The local bandwidth is decreased, and the leading slope of $N_{\boldsymbol{r}}(E)$ around $E \approx 0$ fluctuates, indicating renormalized Fermi velocities in the neighborhood of the apex. In panels Fig. 3(d) and 3(e) we plot the real-space distribution of the LDOS at representative energies around the Dirac point, showing that the charge density is mostly localized in the apex,

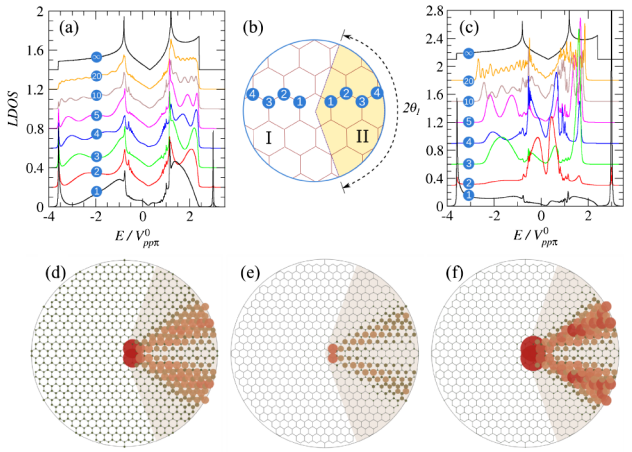

FIG. 3 (color online). LDOS close to the apex of a CS with $\varepsilon = 0.3$, in the regions I (a) and II (c), and at specific lattice positions, as specified in panel (b) The curves in (a),(c) were vertically shifted for clarity. In (d)–(f) we show the LDOS in real-space for selected energies: $E/V^0_{pp\pi} = -0.1, 0.3, 0.4$. More detailed plots are available in [24].

albeit with a "leak" along two rays that are at an angle $\approx 24°$ with the axis of symmetry of the CSs, coinciding with the two zero curvature generators in the entire conical surface (1), and show clearly the role of curvature-induced confinement [24]. We also always see signals of "magnetic" oscillations around the Dirac point, as shown in Fig. 3(a) [32]. Even though these studies are carried out with zero magnetic field, the presence of these locally varying fictitious fields is expected to influence Landau level quantization under a real magnetic field.

CSs have potential to markedly affect electronic properties and transport in wrinkled graphene. They contribute a quasi linear-in-density conductivity, and might even limit mobility in suspended samples at low temperatures, even in the dilute limit. But we just touched the surface of possibilities. We did not consider the anisotropy in the transport calculations, but it is likely to play a role in situations like Fig. 1(b), where a strong alignment might lead to coherent scattering. In addition, σ-π rehybridization can lead to important enhancement of spin-orbit coupling [33]. In suspended samples, curvature-induced disordered flux might be dominant and thus explain why the quantum Hall effect in four-terminal suspended samples is so elusive. Our calculations suggest the possibility of testing these effects by inducing CSs on demand exploring shear, or the anomalous thermal expansion of graphene [2]. Moreover, our findings significantly tally with recent experiments showing a tendency for charge trapping, midgap states, and reduced conductance near wrinkles in graphene [34]. Such strong impact of singular deformations on the electronic system can pave new avenues of interplay between structure and electronics. Graphene, as seen, has clear and unprecedented advantages, insofar as both its mechanical response and electronic structure are easily and accurately modeled down to the atomic level.

A. H. C. N acknowledges the partial support of the U.S. DOE under grant DE-FG02-08ER46512, and ONR grant MURI N00014-09-1-1063. H. L. and L. M acknowledge the support of the Harvard-NSF MRSEC and L. M acknowledges support from the MacArthur Foundation.

*vpereira@bu.edu
lm@seas.harvard.edu.

[1] Jannik C. Meyer *et al.*, Nature (London) **446**, 60 (2007).
[2] W. Bao *et al.*, Nature Nanotech. **4**, 562 (2009).
[3] S. Stankovich *et al.*, Carbon **45**, 1558 (2007).
[4] E. Stolyarova *et al.*, Proc. Natl. Acad. Sci. U.S.A. **104**, 9209 (2007).
[5] M. Ishigami *et al.*, Nano Lett. **7**, 1643 (2007).
[6] V. Geringer *et al.*, Phys. Rev. Lett. **102**, 076102 (2009).
[7] S. Bae *et al.*, Nature Nanotech. **5**, 574 (2010).
[8] P. Sutter, J. T. Sadowski, and E. Sutter, Phys. Rev. B **80**, 245411 (2009).
[9] L. D. Landau and E. M. Lifshitz, *Theory of Elasticity* (Pergamon, New York, 1986), 3rd ed.
[10] C. Lee *et al.*, Science **321**, 385 (2008).
[11] E. Cerda *et al.*, Proc. Natl. Acad. Sci. U.S.A. **101**, 1806 (2004).
[12] E. Cerda and L. Mahadevan, Phys. Rev. Lett. **80**, 2358 (1998).
[13] E. Cerda and L. Mahadevan, Proc. R. Soc. A **461**, 671 (2005).
[14] K. Bolotin *et al.*, Solid State Commun. **146**, 351 (2008).
[15] G. Li, A. Luican, and E. Y. Andrei, Phys. Rev. Lett. **102**, 176804 (2009).
[16] X. Du *et al.*, Nature (London) **462**, 192 (2009).
[17] K. Bolotin *et al.*, Nature (London) **462**, 196 (2009).
[18] A. H. Castro Neto *et al.*, Rev. Mod. Phys. **81**, 109 (2009).
[19] Vitor M. Pereira, A. H. Castro Neto, and N. M. R. Peres, Phys. Rev. B **80**, 045401 (2009).
[20] R. M. Ribeiro *et al.*, New J. Phys. **11**, 115002 (2009).
[21] Vitor M. Pereira and A. H. Castro Neto, Phys. Rev. Lett. **103**, 046801 (2009).
[22] F. Guinea, M. I. Katsnelson, and A. K. Geim, Nature Phys. **6**, 30 (2010).
[23] M. R. Falvo *et al.*, Nature (London) **389**, 582 (1997); D. Bozovic *et al.*, Appl. Phys. Lett. **78**, 3693 (2001).
[24] See supplementary material at http://link.aps.org/supplemental/10.1103/PhysRevLett.105.156603.
[25] L. Mahadevan and S. Rica, Science **307**, 1740 (2005).
[26] E.-A. Kim and A. H. C. Neto, Europhys. Lett. **84**, 57007 (2008).
[27] A. Isacsson *et al.*, Phys. Rev. B **77**, 035423 (2008).
[28] This choice of $V_{ppx} \propto 1/d^2$ is not at all restrictive, since a leading order expansion will be performed for d.
[29] We use $V_{pp\pi}(a_0) = 3$ eV, $V_{pp\sigma}(a_0) = 1.7V_{pp\pi}(a_0)$, $V_{pp\pi}(\sqrt{3}a_0) = 0.1V_{pp\pi}(a_0)$, $V_{pp\sigma}(\sqrt{3}a_0) = 0.1V_{pp\sigma}(a_0)$.
[30] D. S. Novikov, Phys. Rev. B **76**, 245435 (2007).
[31] I. S. Gradshteyn and I. M. Ryzhik, *Table of Integrals, Series, and Products* (World Scientific, Singapore, 1965), 4th ed.
[32] The unrelaxed surface has no in-plain strain, but the 3D interatomic distances in the curved lattice do change.
[33] A. H. Castro Neto and F. Guinea, Phys. Rev. Lett. **103**, 026804 (2009).
[34] K. Xu, P. Cao, and J. R. Heath, Nano Lett. **9**, 4446 (2009).
[35] Courtesy of A. K. Geim and C. N. Lau, respectively.